

# IndoQCT: A PLATFORM FOR AUTOMATED CT IMAGE QUALITY ASSESSMENT

Choirul Anam<sup>1</sup>, Ariij Naufal<sup>1</sup>, Wahyu S. Budi<sup>1</sup>, Heri Sutanto<sup>1</sup>, Freddy Haryanto<sup>2</sup>, Geoff Dougherty<sup>3</sup>

<sup>1</sup>Department of Physics, Faculty of Sciences and Mathematics, Diponegoro University, Jl. Prof. Soedarto SH, Tembalang, Semarang 50275, Central Java, Indonesia

<sup>2</sup>Department of Physics, Faculty of Mathematics and Natural Sciences, Bandung Institute of Technology, Bandung, West Java, Indonesia

<sup>3</sup>Department of Applied Physics and Medical Imaging, California State University Channel Islands, Camarillo, CA 93012, USA

*Abstract*— The quality control (QC) procedure of computed tomography (CT) is an important task to be regularly performed. It consists of daily, monthly, and annual tasks. Each procedure can be time-consuming. Manual QC can take many hours. Manual measurement of image quality parameters can also lead to a bias due to the subjectivity of examiners. IndoQCT answers these challenges by being automatic, fast, objective, and accurate. Unlike some existing software that can only be used on one type of phantom and with limited parameters, IndoQCT can be used to evaluate CT image quality using various phantoms and numerous parameters. In this report, the basic workflow of IndoQCT to automatically evaluate CT image quality on the American College of Radiology (ACR) phantom was assessed. IndoQCT provides a total of 9 main tabs, covering various image quality parameters, namely: CT number (water), CT number of multiple objects, noise, spatial resolution, low contrast, slice thickness, laser alignment, distance accuracy, and gantry tilt. As a tool for productive QC procedures in health facilities, IndoQCT can increase the efficiency of QC.

*Keywords*— computed tomography, QC, image quality, automatic

## IV. INTRODUCTION

Quality control (QC) procedures on X-ray machines, especially computed tomography (CT) scanners, are essential to maintain the performance of the machine over time in order to achieve an accurate diagnosis and to deliver best treatment for patients. Medical personnel carry out routine QC procedures covering the mechanical aspects, output dose, and image quality [1]. Scanner performance is evaluated using a series of specific procedures using dedicated phantoms.

Evaluation of CT image quality can be carried out using manual methods. They mostly involve placing regions of interest (ROI) on target objects to measure certain parameters. The manual method is mainly for basic parameters that do not require complicated mathematical operations. Unfortunately, it can give rise to variability between users, and it is time-consuming [2]. Several automatic tools have been introduced to overcome this problem, especially for measuring advanced Fourier-based image quality parameters, such as the modulation transfer

function (MTF) and the noise power spectrum (NPS) [2-5].

With automated QC software, two main problems can arise, namely transparency and comprehensiveness. Paid software generally does not include complete and transparent documentation, and the algorithm for the automated procedures is proprietary. You are not purchasing the software but only paying to use it. The user is not able to configure/modify the measurement parameters to fit the specific image conditions. It is highly preferable to be able to create an optimal user-customized framework that can be configured in a user-friendly manner according to the specific conditions. With regard to comprehensiveness, although some open-source software provides documentation transparency, the software are limited and can only be applied to one dedicated phantom type, such as the Catphan (The Phantom Laboratory, Salem, USA) or ACR (Gammex Inc, Middletown, WI, USA) [2,6]. Since there are many types of QC phantoms on the market, especially built-in phantoms, the limited coverage of this software will limit easy access for many CT centers having different types of phantoms. Therefore, availability of a software that can be used on different types of phantom is important.

Based on these problems, we developed a software platform called IndoQCT. IndoQCT attempts to address these issues by integrating automated methods for CT image quality evaluation for the many types of phantoms available on the market. In this report, however, we will only demonstrate the basic workflow for common image quality parameters on the ACR 464 phantom.

## V. METHODS

### 2.1 ACR 464 phantom

The ACR 464 phantom consists of 4 modules for measurement of various image quality parameters. The appearance of each module is shown in Figure 1. Table 1 shows the details of the modules and their roles in measuring image quality parameters along with their tolerance limits.

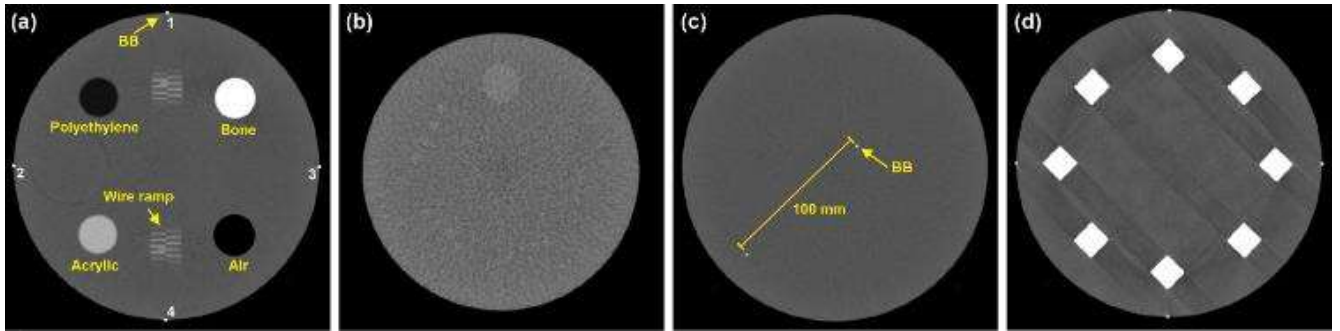


Fig. 1 Images of ACR phantom module (a) #1, (b) #2, (c) #3, and (d) #4.

Table 1 Image quality parameters on each module of ACR phantom

Module	Parameter	Tolerance limit
#1	CT number of multiple objects	<ul style="list-style-type: none"> <li>• Air (-970 to -1005 HU)</li> <li>• Polyethylene (-107 to -84)</li> <li>• Solid water (-7 to +7 HU)</li> <li>• Acrylic (110 to 135 HU)</li> <li>• Bone (850 to 970 HU)</li> </ul>
	CT number linearity	-
	Alignment	$\Delta \text{ laser} \leq \text{minimum slice thickness}$
	Slice thickness	$\Delta \text{ slice thickness} \leq 0.5 \text{ mm}$
#2	TTF*	-
	Low contrast (visual) CNR**	Minimum size $\leq 6 \text{ mm}$ CNR $\geq 1$
#3	CT number (water)	$-7 \text{ HU} \leq \text{CT number} \leq 7 \text{ HU}$
	CT number uniformity	$\leq 5 \text{ HU}$
	Noise	-
	Noise uniformity	Uniformity $\leq 2 \text{ HU}$
	NPS***	-
	Distance accuracy	-
	Gantry tilt	-
#4	Point MTF****	$10\% \text{ MTF} \geq 0.5 \text{ mm}^{-1}$
	Edge MTF	$10\% \text{ MTF} \geq 0.5 \text{ mm}^{-1}$
#4	Spatial resolution (visual)	Line pair $\geq 0.5 \text{ lp/mm}$

\*) TTF is task transfer function

\*\*) CNR is contrast to noise ratio

\*\*\*) NPS is noise power spectrum

\*\*\*\*) MTF is modulation transfer function

## 2.2 IndoQCT main architecture

### 2.2.1 Backend structure

IndoQCT was built using Python 2.7.9 with the PyQt5 Graphical User Interface (GUI) platform. To read and access Digital Imaging and Communications in Medicine (DICOM) images, IndoQCT used the Pydicom library [7]. Through the interface, the user can execute the automatic methods provided. The main matrix operation implemented is Numpy [8]. For the backend process, IndoQCT employed image processing modules, such as scikit-image [9], scipy [10], and Open-CV. For each parameter measurement, IndoQCT processes different functions, based conditionally on the type of phantom that can be selected.

### 2.2.2 Frontend structure

The IndoQCT GUI has a similar layout to many DICOM viewer software. Figure 2 shows the layout of the GUI components of IndoQCT. The main features for image quality measurement were embedded into the main tabs on the right side of the main viewer. The 9 tabs are based on their parameter categories, from top to bottom, namely CT number (water), CT number of multiple objects, noise, spatial resolution, low contrast detectability, slice thickness, alignment, distance accuracy, and gantry tilt. The tabs were sorted based on the frequency of their use in field scenarios. In each tab, it can be divided into sub-tabs according to its specific parameters, such as the CT number tab consisting of accuracy, uniformity, homogeneity, histogram, profile, and patient sub-tabs. However, in this report, we will only briefly elaborate on the parameters that are commonly assessed in QC procedures.

In each tab, the components were carefully organized so that both input parameters and results can be understood intuitively. Input parameters are useful for configuring the measurement parameters according to the image conditions to be evaluated. By default, the input parameters are set to ideal values that work for most images. The "Calculate" button is provided to trigger the automatic algorithm on each tab. After the automatic algorithm is activated, the results are printed in the results column on the right side. More in-depth details for each automatic measurement will be discussed in the image quality parameters section.

For each image quality measurement, the results are compared to the standards provided (Table 1). The evaluation according to the standard is automatically accomplished in the standards section (PASSED/FAILED). Several sets of configurations were included according to guidelines from regulatory agencies, such as Nuclear Energy Regulatory Agency of Indonesia (BAPETEN) [11], International Atomic Energy Agency (IAEA) [12], American College of Radiology (ACR), American Association of Physicists in Medicine (AAPM), and user baseline.

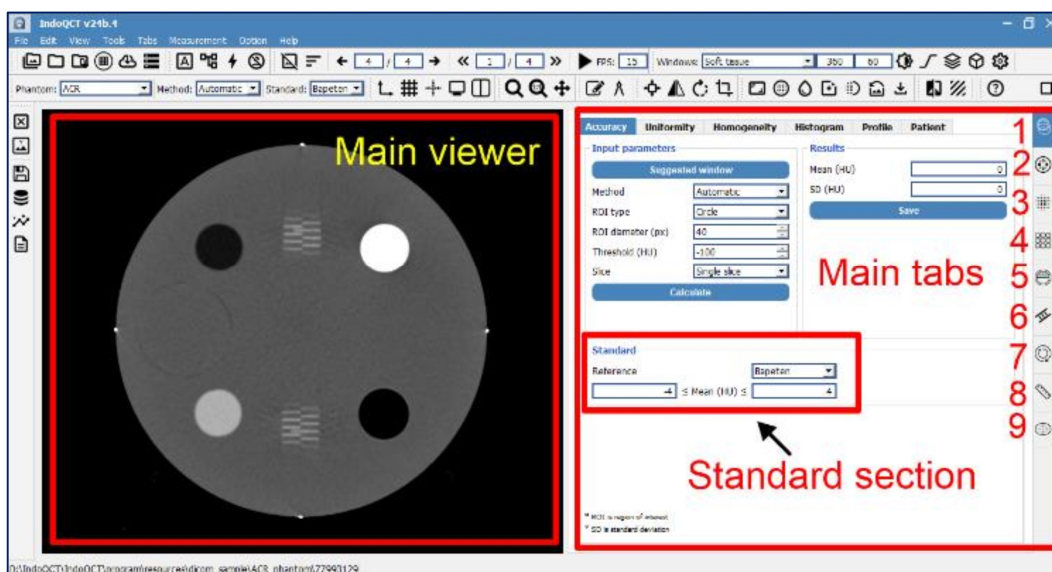


**Fig. 2** The graphical user interface of IndoQCT. It consists of a main viewer, main tabs, and standard sections. A total of 9 main tabs for the measurement of different image quality parameters is provided: (1) CT number of water, (2) CT number of multiple objects, (3) Noise, (4) Spatial resolution, (5) Low contrast detectability, (6) Slice thickness, (7) Laser alignment, (8) Distance accuracy, and (9) Gantry tilt

### 2.3 Image quality parameters

#### 2.3.1 CT number of water

In the tab of CT number of water, sub-tabs of CT number accuracy and CT number uniformity can be chosen. IndoQCT segments the phantom and determines its centroid coordinates. A circular ROI of 2 cm in diameter is placed at the centroid. Figure 3a shows the ROI positioning for CT number of water measurement on the ACR phantom. CT number accuracy is measured by averaging the pixel intensities in Hounsfield units (HU) of the ROI. For measuring CT number uniformity, IndoQCT places 5 ROIs, namely in the center of the phantom and at the periphery (3, 6, 9, 12 o'clock). Figure 3b shows the placement of each ROI in the CT number uniformity measurement. The peripheral ROIs were 3 cm away from the edge of the phantom. CT number uniformity is measured as the largest difference between the peripheral ROI and the central ROI, as defined by equation (1).

$$U_{CT} = \max(ROI_p - ROI_c) \quad (1)$$

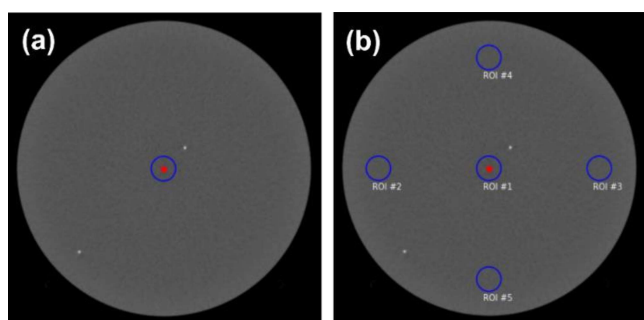


**Fig. 3** Automatic measurements of CT number of water on ACR phantom. (a) CT number accuracy, and (b) CT number uniformity.

#### 2.3.2 CT number of multiple objects

In the tab of the CT number of multiple objects, a feature for automatically measuring the CT number of objects with different densities was provided. The CT number of multiple objects is automatically obtained by detecting objects with varying CT numbers, as listed in the phantom manual book. ROIs are automatically drawn on the target objects to obtain the average CT number of each material (Figure 4a). The measurement results for each material are then displayed in the result column, along with its density and reference. As an extension of this measurement, the linearity of the CT number of multiple objects can be calculated by determining the regression coefficient between the CT number and the density of each material (Figure 4b) [13-15].

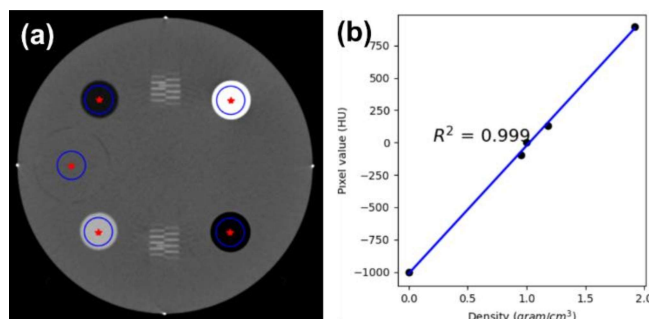


**Fig. 4** Measurement of CT number of multiple objects on ACR phantom. (a) ROI placement on 5 different materials, (b) Determining the linearity.

#### 2.3.3 Noise

In the tab of noise, noise accuracy is measured using a process similar to CT number accuracy (Figure 3a), by

placing the ROI in the center of the phantom. Noise is measured by calculating the standard deviation of the pixels within the ROI [16]. In addition to noise accuracy, noise uniformity is also evaluated to ensure that noise levels are uniform across regions. Noise uniformity is measured using a process similar to CT number uniformity (Figure 3b), by placing 5 ROIs at the center and at the periphery (3, 6, 9, 12 o'clock). Noise uniformity is defined as the maximum difference between maximum noise in one ROI and minimum noise in the one of the remaining ROIs, shown by equation (2).

$$U_{\sigma} = \max(\sigma) - \min(\sigma) \quad (2)$$

Noise texture characterized by NPS is also available in a specific sub-tab. NPS measurement is performed by drawing a number of square ROIs (i.e., 1, 3, or 5) on a homogeneous region in the phantom (Figure 5a). Then, the two-dimensional (2D) NPS is obtained using equation (3).

$$NPS_{(u,v)} = \frac{d_x d_y}{N_x N_y} \cdot |\mathcal{F}[I(x,y) - P(x,y)]|^2 \quad (3)$$

where  $u$  and  $v$  are the spatial frequencies in the X- and Y-axes.  $d_x$  and  $d_y$  are the pixel sizes, and  $N_x$  and  $N_y$  are the number of pixels in the X- and Y-axes in the ROI.  $\mathcal{F}$  represents the Fourier transform,  $I$  represents the pixel value, and  $P$  is the polynomial fit of  $I$ .

One-dimensional (1D) NPS (NPS(f)) is obtained by radially averaging the two-dimensional (2D) NPS. The peak and average frequencies are determined from the 1D NPS [17,18]. Figure 5b shows an example of 1D NPS obtained on an ACR phantom image. An option for a polynomial fit of the 1D NPS with a maximum of 11-th order is provided, as proposed by [19,20].

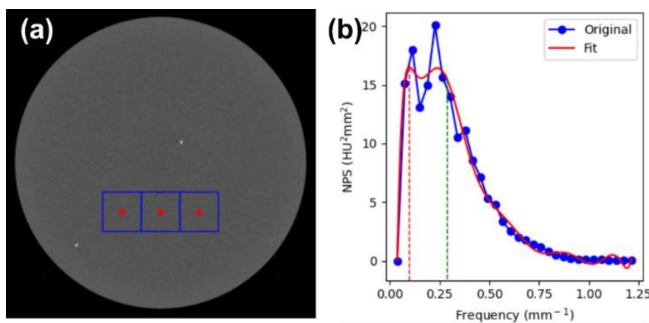


**Fig. 5** Automatic measurements of NPS on ACR phantom. (a) ROI placement on homogeneous area, and (b) Example of 1D NPS with 11<sup>th</sup> order polynomial fit.

### 2.3.4 Spatial resolution

In the tab of the spatial resolution, several sub-tabs for various methods of measuring spatial resolution are provided. Spatial resolution can be determined using visual observation. The phantom images used generally display

line pairs. Figure 1d shows an image of the line pairs displayed at a window width of 100 and window level of 1100, as recommended by ACR. To minimize user variability in visual observation, IndoQCT provides an automated method. The ACR phantom image is processed to obtain a standard deviation (SD) map. The objects for a specific SD criteria are identified above the threshold to determine the resolvable objects (Figure 6a).

In addition to using line pairs, spatial resolution can also be measured through the modulation transfer function (MTF). In IndoQCT, Point MTF is one of the options to characterize spatial resolution [21-23]. In the ACR phantom module #3, there are 2 point objects that can be used for Point MTF measurement. One of the point objects is detected using simple segmentation to obtain its coordinates. A ROI is drawn at the coordinates of the point object (Figure 6b). The resulting array is summed according to the selected option (e.g. X-axis or Y-axis, depending on the desired resolution dimension), to generate a point spread function (PSF). The PSF is automatically zeroed and normalized (Figure 6c). A Fourier transform is performed on the PSF to generate an MTF curve (Figure 6d). The 10% and 50% MTFs are displayed in IndoQCT.

In many cases, Point MTF produces fluctuating curves due to high noise. Edge MTF provides a reliable alternative option [24,25]. In the ACR phantom, Edge MTF is obtained by collecting the phantom edge response (edge spread function, ESF), which is differentiated to generate a line spread function (LSF). The LSF is then Fourier transformed to generate the MTF curve. Figure 6e shows the ROI placement for edge MTF measurement. Since the edge response was obtained from the phantom edge, the potential for fluctuation is always present. To anticipate disturbances, several options to correct the ESF, such as tail replacement, homogenization, mirroring, and single logistic fit are provided. Users can select these options according to their needs.

TTF is an image quality parameter characterizing spatial resolution as a function of contrast and local noise. TTF plays an important role in describing the spatial resolution of CT systems in non-linear and shift-variant iterative reconstruction. TTF is analogous to MTF. However, when reporting TTF, contrast and local noise are also reported [26]. To measure TTF, circular disk-shaped inserts made of various materials are required. In the ACR phantom, 4 circular objects are available, namely bone, air, acrylic, and polyethylene. These four objects are automatically detected to identify their coordinates. A circular ROI is placed on each object coordinate and the object edge responses obtained radially. The ESF is calculated as the average of the edge response samples. The rest of the process is similar to those for edge MTF. Figure 7 shows an example of TTF measurement in IndoQCT.



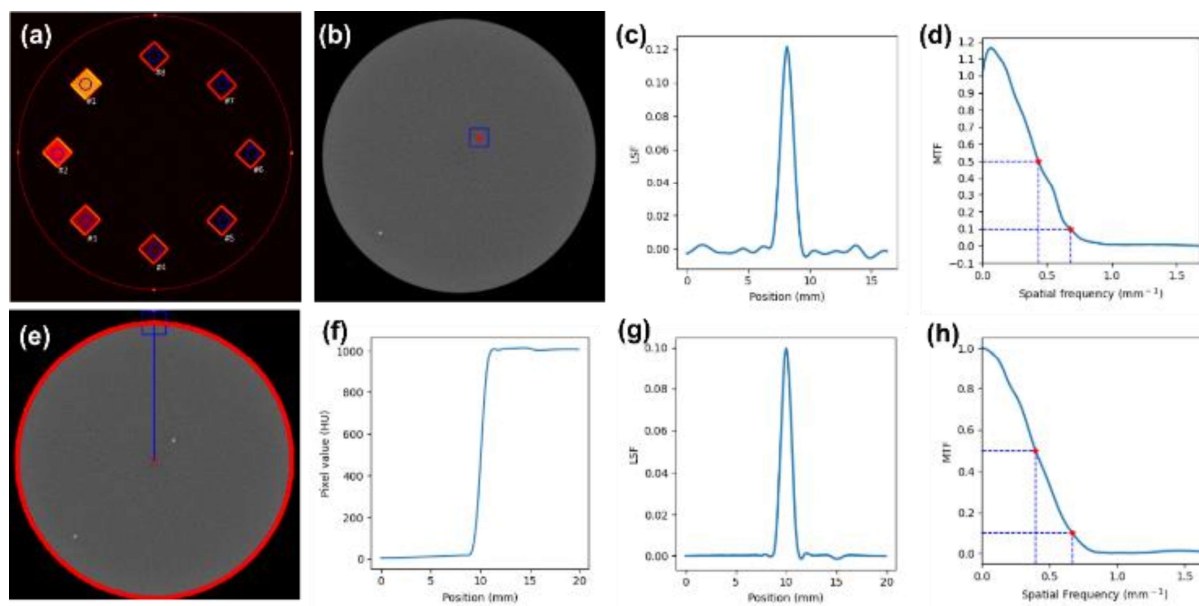


**Fig. 6** Automatic measurements of spatial resolution on ACR phantom. (a) SD map with line pair annotated, (b) ROI placement on point object, (c) Example of zeroed and normalized PSF, (d) MTF curve derived from (c), (e) ROI placement on phantom's edge, (f) Example of ESF obtained, (g) LSF derived from (f), and (h) MTF curve derived from (g).

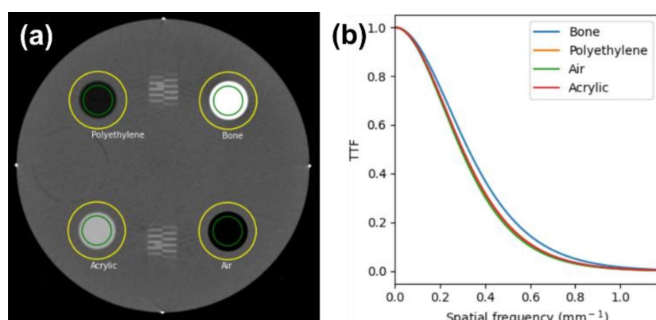


**Fig. 7** Automatic measurements of TTF on ACR phantom. (a) ROI placement on 4 circular objects, (b) Example of TTF curves from various materials.

### 2.3.5 Low contrast detectability

In the tab of the low contrast, visual low contrast detectability and contrast-to-noise ratio (CNR) assessments are provided. Low contrast detectability can be visually observed by a human observer. In the ACR phantom, a low contrast module consisting of a series of cylinders with various diameters is provided. An automated low contrast detectability assessment workflow is available in IndoQCT. After opening a suitable image, the user can set the window width and window level to 100 and 100, as recommended by ACR, using a button provided. By doing so, the appearance of low contrast objects will become clearer for identification. Using an automated method, IndoQCT identifies the coordinates of each target object through a reference object (a 25 mm diameter cylinder) to place a ROI on each target, in addition to placing a ROI in the center of the phantom for the background. The CNR of each object against the

background at the center of the phantom is calculated using equation (4). Using the set CNR threshold, the CNR of the object series that is not less than the threshold is considered resolvable against the background. The smallest object series that is still resolvable indicates low contrast detectability of the image [27]. Figure 8a shows the detection result of the low contrast object series on the ACR phantom.

In addition to visual observation, CNR is also widely considered to describe the ability of a CT system to emphasize low contrast lesions. IndoQCT provides an automated tool for CNR measurement on a phantom. In CNR measurement, two ROIs are drawn on the object (25 mm diameter cylinder) and background (Figure 8b)., Segmentation of the phantom and the low contrast object is performed to obtain the center coordinates of both. CNR is then calculated using equation (4).

$$CNR = \frac{|I_{object} - I_{background}|}{\sigma} \quad (4)$$

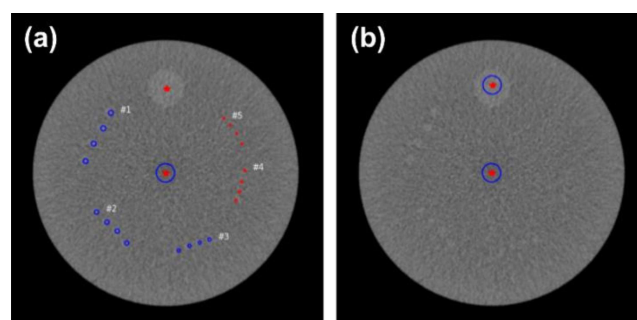


**Fig. 8** Automatic measurements of low contrast detectability on ACR phantom. (a) Visual observation of series of objects (blue circles indicate

resolvable objects, and red circles indicate non-resolvable objects), (b) CNR measurements.

### 2.3.6 Slice thickness

On the tab of the slice thickness, slice thickness can be automatically measured. In the ACR phantom, a pair of wire ramps with a spacing of 0.5 mm each is provided. Slice thickness measurement is performed by enumerating the number of wires visible on the axial image. To minimize the subjectivity of manual observation, IndoQCT provides an automated method [28]. Two profile lines are drawn on the left and right sides so that they crossed both ramps. The pixel profiles from both sides are then normalized. The number of peaks is calculated as a representation of the number of enumerated objects. Slice thickness in mm is measured by multiplying the object count by the distance between them (0.5 mm). Figure 9 displays the ROI placement of the automatic slice thickness measurement on the ACR phantom.

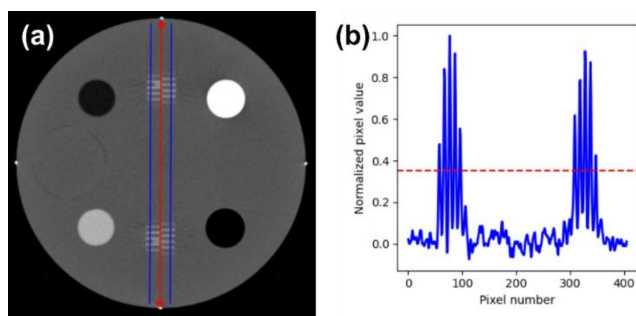


**Fig. 9** Automatic slice thickness on ACR phantom. (a) Two profile lines placed on wire ramps, (b) Example of object counting from their normalized pixel profile. Red line indicates the threshold value and it can be set by user.

### 2.3.7 Laser alignment

Laser alignment is the mechanical aspect test of CT. Laser alignment as a tool helping to locate the phantom on the iso-center. The accuracy of the phantom placement at the iso-center directly influences the image quality and the dose distribution within it. In the ACR phantom, several markers (at 3, 6, 9, 12 o'clock) to evaluate alignment are provided. These marker objects exist in modules #1 and #4, shown in Figure 1a and 1d. Through laser alignment measurement, the accuracy of phantom positioning in the X, Y, and rotational axis directions in degrees can be determined. IndoQCT segments the alignment marker objects and measures their precision against the image's central axis [29]. Figure 10 shows the automatic detection of the alignment measurement.

### 2.3.8 Distance accuracy

ACR phantom provides a module for distance accuracy measurement, in the form of two point objects at a distance of 100 mm in module #3 (Figure 1c). This parameter

evaluates the accuracy of CT reconstruction, especially in terms of geometry in XY coordinates. IndoQCT provides a feature for automatic measurement of distance accuracy in the distance tab. An example of the detection results of the two point objects measuring distance accuracy on the ACR phantom is shown in Figure 11.

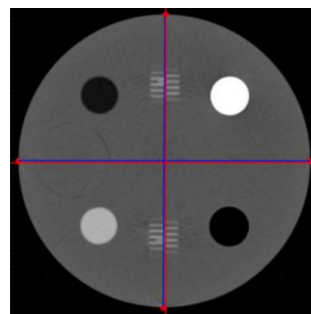


**Fig. 10** Automatic phantom alignment measurements on ACR phantom module #1. The red lines indicate the lines through the center of the image, and the blue lines connect four markers.

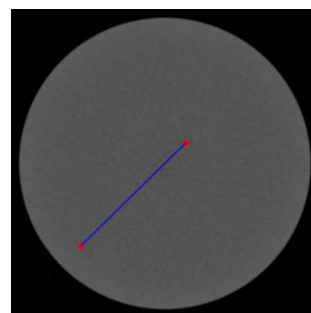


**Fig. 11** Automatic measurements of distance accuracy on the ACR phantom.

### 2.3.9 Gantry tilt

Gantry tilt measurements can be easily and automatically done on the axial image using IndoQCT. By segmenting the phantom object, the lateral (LAT) and anterior-posterior (AP) diameters can be obtained. The tilt angle ( $\theta$ ) is calculated using equation (5) [30]. The measurement results are compared with the gantry tilt information that can be accessed from the DICOM tags, using the (0018,1120) Gantry/Detector Tilt tag. Figure 12 shows the detection of LAT and AP diameters on the ACR phantom.

$$\theta = \cos^{-1} \left( \frac{LAT}{AP} \right) \quad (5)$$

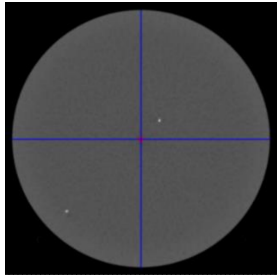


Fig. 12 Automatic gantry tilt measurement on ACR phantom.

VI. RESULTS

Table 3 shows a summary of the results of the ACR phantom image quality assessment from the 3 scanners automatically using IndoQCT. In some measurements, the results were evaluated automatically using the standards set by ACR. Of the various measurement parameters, laser alignment showed results that did not meet the standard, especially in scanner #1, where the delta x and y exceeded the 2 mm tolerance limit. This indicates an off-center phantom position up and to the right. In the measurement of CT number of multiple objects, IndoQCT can detect the target objects correctly and obtain the desired measurement results. The CT numbers for the bone insert were above the upper recommended range for scanners #2 and #3. The NPS measurement describes the noise distribution at different frequencies, indicating a difference in texture between the 3 scanners despite them having similar noise levels. In the spatial resolution measurement using several methods, the measurement results showed close agreement between line pair assessment, point, and edge MTF.

2.4 Initial assessment

As an initial study, various parameters of image quality of ACR phantom scanned from 3 scanners were measured. The acquisition parameters for the 3 scanners are shown in Table 2. Measurement of image quality parameters was performed using the default configuration of IndoQCT.

Table 2 Acquisition parameters of ACR phantom image from 3 different scanners

Parameter	Scanner #1	Scanner #2	Scanner #3
Scanner type	GE Discovery LS	GE Revolution ACTs	GE Revolution EVO
Scan mode	Axial	Axial	Axial
Tube current (mA)	250	200	120
Tube voltage (kV)	120	120	120
Slice thickness (mm)	5	10	5
Field of view (mm)	240	250	233
Filter type	Body	Head	Head

VII. DISCUSSION

As a tool in carrying out QC procedures in productive healthcare facilities, IndoQCT is reliable and provides a simple workflow to run. This is demonstrated from the measurements in the Results section, where all parameters in every dataset were comprehensively evaluated in only about 5 minutes.

Table 3 Summary of image quality assessment for ACR phantom image from 3 different scanners

Main parameter	Sub parameter	Scanner #1	Scanner #2	Scanner #3	Standard
CT number of water	Accuracy (HU)	-1.0	-2.2	-2.0	-7 to +7
	Uniformity (HU)	3.3	0.8	1.6	≤ 5
CT number of multiple object	Accuracy (HU)				
	• Air	• -998.8	• -978.0	• -993.5	• -970 to -1005
	• Polyethylene	• -91.8	• -99.5	• -97.2	• -107 to -84
	• Solid water	• -1.0	• -1.7	• -1.3	• -7 to +7
	• Acrylic	• 120.9	• 118.3	• 119.8	• 110 to 135
Noise image	• Bone	• 916.7	• 1052.4	• 980.0	• 850 to 970
	Linearity (R <sup>2</sup> )	0.9984	0.9906	0.9958	-
	Noise level (HU)	5.3	2.47	3.16	-
	Uniformity (HU)	1.0	0.4	0.3	-
	NPS: Peak frequency (mm <sup>-1</sup> )	0.29	0.06	0.23	-
Spatial resolution	NPS: Average frequency (mm <sup>-1</sup> )	0.33	0.26	0.29	-
	Automatic assessment on line pair object (mm <sup>-1</sup> )	0.70	0.60	0.70	0.50
	Point MTF: 10% MTF (mm <sup>-1</sup> )	0.68	0.63	0.70	0.50
	Edge MTF: 10% MTF (mm <sup>-1</sup> )	0.62	0.58	0.78	0.50
	10% TTF (mm <sup>-1</sup> )				
Low contrast detectability	• Air	• 0.69	• 0.60	• 0.76	-
	• Polyethylene	• 0.67	• 0.62	• 0.73	-
	• Acrylic	• 0.73	• 0.60	• 0.74	-
	• Bone	• 0.69	• 0.57	• 0.90	-
	Automatic assessment with various size (mm)	4	3	5	≤ 6
Slice thickness	CNR	1.3	2.6	1.7	≥ 1
	Slice thickness (mm) / Difference (mm)	5.2 / 0.2	9.8 / 0.2	4.8 / 0.2	Difference ≤ 1.5

Laser alignment	• x-axis (mm)	• <b>4.9</b>	• -0.5	• <b>1.8</b>	• $\leq 2$
	• y-axis (mm)	• <b>8.4</b>	• 0.8	• 0.4	• $\leq 2$
Distance accuracy	Distance accuracy (mm) / Difference (mm)	100.1 / 0.1	100.1 / 0.1	100.1 / 0.1	Difference $\leq 1$
Gantry tilt	Gantry tilt (°)	0.0	0.0	0.0	-

\*Bold shows FAILED values.

## VIII. DISCUSSION

As a tool in carrying out QC procedures in productive healthcare facilities, IndoQCT is reliable and provides a simple workflow to run. This is demonstrated from the measurements in the Results section, where all parameters in every dataset were comprehensively evaluated in only about 5 minutes.

This study only showed the measurement of various parameters on the ACR phantom using IndoQCT. IndoQCT itself can measure various parameters from many other phantoms, such as Catphan, AAPM CT performance, GE, Siemens, Toshiba, Philips, Hitachi, and Neusoft. With the many phantom options in IndoQCT, it helps healthcare facilities having different phantoms. The automated method in IndoQCT improved efficiency for the evaluation of a set of image quality parameters. Moreover, automatic detection reduces manual user interventions and leads to more objective results. IndoQCT can also save the image quality evaluation in the database. This is very useful for observing shifts in quality trends over time, leading to its potential for research and monitoring.

Using IndoQCT, medical personnel can develop a report in a pdf file from the results of QC tests conducted periodically. This feature helps medical personnel to report QC results to related parties and to physically archive data. It is noted that the image quality parameters discussed in this report were also limited to the most commonly evaluated parameters. This report did not include advanced parameters such as CT number homogeneity, noise homogeneity, z-MTF, and so on.

One of the challenges for automation software such as IndoQCT is its robustness to various image conditions. Object detection algorithms that use thresholding techniques or other image processing operations may suffer when applied to images with extreme conditions, i.e. high noise or prominent artefacts. Suboptimal object detection may result in mis-positioning of the ROI, leading to measurement inaccuracies. Therefore, in addition to the automatic method, the option of a manual method is also provided. The workflow of the manual method depends on the type of phantom and the image quality parameters to be measured. For example, in Figure 2, in the parameter input section, a measurement method option was provided for each parameter. When the manual option is activated, the user can manually place the ROI on the desired object, and proceed to the calculation as usual. Another example is the slice thickness measurement on the ACR phantom, where the manual method only requires the user to enumerate the wire

objects and select the number in the user interface (UI) provided. IndoQCT is still at the development stage. Improvements are needed to assess new types of phantoms, as well as new methods for CT image evaluation.

## IX. CONCLUSIONS

IndoQCT was used to automatically evaluate the image quality of the ACR phantom. The image quality parameters were CT number (water), CT number of multiple objects, noise, spatial resolution, low contrast, slice thickness, laser alignment, and distance accuracy. Due to its simple workflow displayed on an intuitive GUI, IndoQCT has the potential to increase the work efficiency of medical personnel for QC procedure.

## ACKNOWLEDGMENT

This work was funded by the Riset Publikasi Internasional Bereputasi Tinggi (RPIBT), Diponegoro University (No. 569-187/UN7.D2/PP/IV/2023).

## REFERENCES

- [1] Roa AM, Andersen HK, Martinsen AC. CT image quality over time: comparison of image quality for six different CT scanners over a six-year period. *J Appl Clin Med Phys.* 2015;16(2):4972. Published 2015 Mar 8. doi:10.1120/jacmp.v16i2.4972
- [2] Karius A, Bert C. QAMaster: A new software framework for phantom-based computed tomography quality assurance. *J Appl Clin Med Phys.* 2022;23(4):e13588. doi:10.1002/acm2.13588
- [3] Greffier J, Barbotteau Y, Gardavaud F. iQMATRIX-CT: New software for task-based image quality assessment of phantom CT images. *Diagn Interv Imaging.* 2022;103(11):555-562. doi:10.1016/j.diii.2022.05.007
- [4] Medical Physics Perth. CT quality inspector (<https://medicalphysicsperth.com/ct-quality-inspector-ctqi>)
- [5] QA Benchmark. AutoQA Plus CT (<http://qabenchmark.com/ct/>)
- [6] Hobson MA, Soisson ET, Davis SD, Parker W. Using the ACR CT accreditation phantom for routine image quality assurance on both CT and CBCT imaging systems in a radiotherapy environment. *J Appl Clin Med Phys.* 2014;15(4):4835. Published 2014 Jul 8. doi:10.1120/jacmp.v15i4.4835
- [7] Mason D. SU-E-T-33: Pydicom: An Open Source DICOM Library. *Med Phys.* 2011;38(Issue6Part10): 3493-3493. doi:10.1118/1.3611983
- [8] Harris CR, Millman KJ, van der Walt SJ, et al. Array programming with NumPy. *Nature.* 2020;585:357-362. doi: 10.1038/s41586-020-2649-2
- [9] van der Walt S, Schönberger JL, Nunez-Iglesias J, et al. scikit-image: Image processing in Python. *PeerJ.* 2014;2:e453. doi:10.7717/peerj.453
- [10] Virtanen P, Gommers R, Oliphant TE, et al. SciPy 1.0: fundamental algorithms for scientific computing in Python. *Nat Methods.* 2020;17(3):261-272. doi:10.1038/s41592-019-0686-2



- [11] Badan Pengawas Tenaga Nuklir. Peraturan Badan pengawas Tenaga Nuklir Nomor 2 Tahun 2018 tentang Uji Kesesuaian Pesawat Sinar-X Radiologi Diagnosik dan Intervensial. Bapeten: Jakarta, Indonesia. 2018.
- [12] INTERNATIONAL ATOMIC ENERGY AGENCY. Quality Assurance Programme for Computed Tomography: Diagnostic and Therapy Applications, IAEA Human Health Series No. 19. IAEA: Vienna. 2012.
- [13] Anam C, Amilia R, Naufal A, Budi WS, Maya AT, Dougherty G. Automated measurement of CT number linearity using an ACR accreditation phantom. *Biomed Phys Eng Express*. 2023;9(1):017002. doi:10.1088/2057-1976/aca9d5
- [14] Anam C, Amilia R, Naufal A, Sutanto H, Dwihapsari Y, Fujibuchi T, Dougherty G. Impact of Noise Level on the Accuracy of Automated Measurement of CT Number Linearity on ACR CT and Computational Phantoms. *J Biomed Phys Eng*. 2023;13(4):353-362. doi:10.31661/jbpe.v0i0.2302-1599
- [15] Anam C, Amilia R, Naufal A, Ali MH. Automatic measurement of CT number in the ACR CT phantom and its implementation to investigate the impact of tube voltage on the measured CT number. *Rad Phys Chem*. 2024;216:111434. doi:10.1016/j.radphyschem.2023.111434
- [16] Anam C, Triadyaksa P, Naufal A, Arifin Z, Muhlisin Z, Setiawati E, Budi WS. Impact of ROI size on the accuracy of noise measurement in CT on computational and ACR phantoms. *J Biomed Phys Eng*. 2022;12(4):359-368. doi:10.31661/jbpe.v0i0.2202-1457
- [17] Anam C, Naufal A, Sutanto H, Adi K, Dougherty G. Impact of iterative bilateral filtering on the noise power spectrum of computed tomography images. *Algorithms*. 2022;15(10):374. doi:10.3390/a15100374
- [18] Setiawan AMB, Anam C, Hidayanto E, Sutanto H, Naufal A, Dougherty G. Comparison of noise-power spectrum and modulation-transfer function for CT images reconstructed with iterative and deep learning image reconstructions: An initial experience study. *Pol J Med Phys Eng*. 2023;29(2):104-112. doi:10.2478/pjmpe-2023-0012
- [19] Greffier J, Si-Mohamed S, Frandon J, et al. Impact of an artificial intelligence deep-learning reconstruction algorithm for CT on image quality and potential dose reduction: A phantom study. *Med Phys*. 2022;49(8):5052-5063. doi:10.1002/mp.15807
- [20] Li Y, Jiang Y, Liu H, et al. A phantom study comparing low-dose CT physical image quality from five different CT scanners. *Quant Imaging Med Surg*. 2022;12(1):766-780. doi:10.21037/qims-21-245
- [21] Anam C, Fujibuchi T, Budi WS, Haryanto F, Dougherty G. An algorithm for automated modulation transfer function measurement using an edge of a PMMA phantom: Impact of field of view on spatial resolution of CT images. *J Appl Clin Med Phys*. 2018;19(6):244-252. doi:10.1002/acm2.12476
- [22] Anam C, Fujibuchi T, Haryanto F, Budi WS, Sutanto H, Adi K, Muhlisin Z, Dougherty G. Automated MTF measurement in CT images with a simple wire phantom. *Pol J Med Phys Eng*. 2019;25(3):179-187. doi:10.2478/pjmpe-2019-0024
- [23] Anam C, Haryanto F, Widita R, Arif I, Dougherty G. An investigation of spatial resolution and noise in reconstructed CT images using iterative reconstruction (IR) and filtered back-projection (FBP). *J Phys: Conf Ser*. 2019;1127:012016. doi:10.1088/1742-6596/1127/1/012016
- [24] Anam C, Ainurrofik N, Sutanto H, Naufal A, Haekal M. Rectangular and radial region of interests on the edge of cylindrical phantom for spatial resolution measurement. *Indonesian J Elec Eng Comp Sci*. 2023;31(2):747-754. doi:10.11591/ijeecs.v31.i2.pp747-754
- [25] Hak EZ, Anam C, Budi WS, Dougherty G. An improvement in automatic MTF measurement in CT images using an edge of the PMMA phantom. *J Phys: Conf Ser*. 2020;1505(1):012039. doi:10.1088/1742-6596/1505/1/012039
- [26] Samei E, Bakalyar D, Boedeker KL, et al. Performance evaluation of computed tomography systems: Summary of AAPM Task Group 233. *Med Phys*. 2019;46(11):e735-e756. doi:10.1002/mp.13763
- [27] Setiawati E, Anam C, Widyasari W, Dougherty G. The quantitative effect of noise and object diameter on low-contrast detectability of AAPM CT performance phantom images. *Atom Indonesia*. 2023;49(1):61-66. doi:10.55981/aij.2023.1228
- [28] Insiano DA, Anam C, Hidayanto E, Naufal A, Maya AT. Optimal Threshold for Automatic Slice Thickness Measurement using Images of the American College of Radiology (ACR) CT Accreditation Phantom. *Int J Sci Res Sci Tech*. 2022;9(6):437-444. doi:10.32628/IJSRST229651
- [29] Anam C, Amilia R, Naufal A, Dougherty G. Algorithm development for automatic laser alignment assessment on an ACR CT phantom and its evaluation of sixteen CT scanners. *Biomed Phys Eng Express*. 2023;9:067002. doi:10.1088/2057-1976/acff76
- [30] Noviliawati R, Anam C, Sutanto H, Dougherty G, Mak'ruf MR. Automatic validation of the gantry tilt in a computed tomography scanner using a head polymethyl methacrylate phantom. *Pol J Med Phys Eng*. 2021;27(1):57-62. doi:10.2478/pjmpe-2021-0008

Contacts of the corresponding author:

Author: Choirul Anam  
 Institute: Diponegoro University  
 Street: Jl. Prof. Soedarto SH, Tembalang  
 City: Semarang, Central Java  
 Country: Indonesia  
 Email: anam@fisika.fsm.undip.ac.id